Proceedings of The Canadian Society for Mechanical Engineering International Congress 2018
CSME International Congress 2018
May 27-30, 2018, Toronto, On, Canada

Effect of Photoacoustic Radar Chirp Parameters on Signal to Noise Ratio

Zuwen Sun
Department of Mechanical Engineering
University of Ottawa
Ottawa, Canada
zsun046@uottawa.ca

Natalie Baddour
Department of Mechanical Engineering
University of Ottawa
Ottawa, Canada
nbaddour@uottawa.ca

Abstract—Continuous wave photoacoustics has been under investigation for more than a decade. Matched-filtering and pulse compression techniques, which use a chirp waveform as input light source, have been implemented into this imaging modality to improve signal to noise ratio (SNR) and resolution. However, the chirp parameters' effects on SNR are still not clear. The theory behind chirp parameters' effects on SNR is discussed in this paper. It is found that in order to get a higher SNR, chirp duration *T* should be maximized, chirp center frequency f_0 should be controlled to make the chirp spectrum overlap with absorber spectrum, and chirp bandwidth Δ should be smaller or equal to the absorber bandwidth.

Keywords-Continuous wave photoacoustics, SNR, chirp

I. INTRODUCTION

Photoacoustic imaging, also called optoacoustic imaging, for biomedical applications has attracted a lot of interest during the past several decades. The principle of this imaging method can be found in recent work [1], [2].

The most common excitation source for photoacoustics has been a pulsed electromagnetic wave [3]–[5]. The key advantage of using a short pulse to irradiate the tissue is that the distribution of heat sources can be directly ascertained from the shape of the photoacoustic response signal [6]. However, the pulsed laser modality is limited by incident energy levels that must meet safety standards for in-vivo tissue imaging [1], as well as the difficulty in generating and detecting very short pulses.

An alternative excitation modality, which uses a continuous incident laser wave, is often referred to as Frequency Domain photoacoustics (FD-PA) where the acoustic wave is generated by periodic modulation of a laser [1], [2], [7]–[11]. More recently, the idea of implementing a pulse compression approach via matched filtering was introduced and investigated [2], [7]–[10], [12]–[14]. This is sometimes referred to as Photoacoustic Radar (PAR). The matched filter approach enables detection of a pre-known signal immersed in Gaussian white noise, therefore a long duration coded waveform with moderate power could potentially replace short high-power pulses.

Signal to Noise Ratio (SNR) is one important aspect to assess the performance of an imaging system. Many theoretical and experimental investigations have been done on the SNR of FD-PA [2], [8], [10], [12]. However, the theory behind optimizing input optical waveform parameters is still not clear. In this paper, the one-dimensional theory of FD-PA will be developed, and the incident wave parameters' effects on SNR will be discussed.

II. 1-D THEORY OF CONTINUOUS WAVE PHOTOACOUSTICS SIGNAL TO NOISE RATIO

Diebold [15] gives a concise explanation of the governing equation for the pressure that results from launching a photoacoustic wave. The governing equation is given by

$$\left[\nabla^2 - \frac{1}{c_s^2}\frac{\partial^2}{\partial t^2}\right] p(\vec{r},t) = -\frac{p_0}{c_s^2} A(\vec{r}) \frac{\partial I(t)}{\partial t} \quad (1)$$

where $p_0 = \frac{\beta c_s^2}{C_p}\mu_a F$ and β is the thermal expansion coefficient, c_s is the speed of sound, C_p is the specific heat, μ_a is the optical absorption coefficient of the chromophore absorber that has been heated by an optical pulse with fluence *F*. $p(\vec{r},t)$ is the pressure of the acoustic wave, a function of space and time. $A(\vec{r})$ is a function of space that describes the geometry of the absorber and $I(t)$ is a function that describes the time dependence of the incident optical pulse.

In one-dimensional model as shown in Figure 1. a), the space variable $\vec{r}$ becomes z. The incident laser waveform $I(t)$ is transmitted from the negative side of z axis, outside of the absorbing medium. The absorber is considered as an infinite sheet with a thickness l. The speed of sound c_s is considered to be the same in all three layers [16]. The pressure response $p(z,t)$ is then detected by a transducer and be sent

to a receiver-filter. The output of the receiver-filter $y(z,t)$ is the final photoacoustic signal.

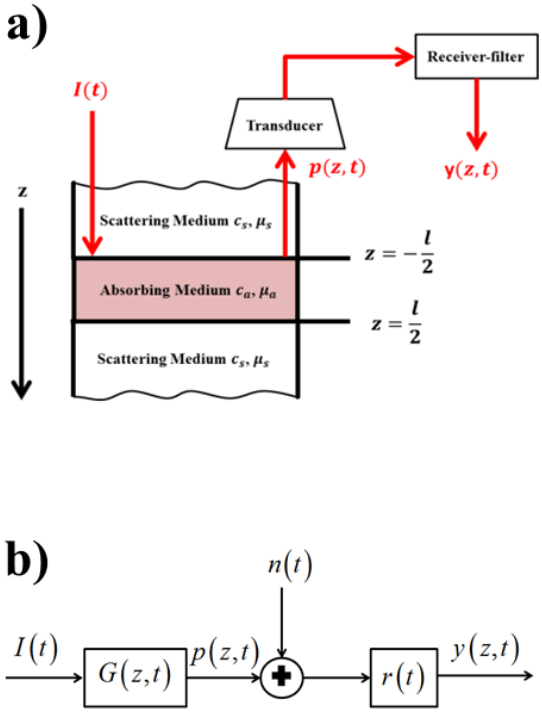

Figure 1. a) Model of absorber and surroundings; b) block diagram

When viewing the system shown in Figure 1. a) as a linear system, as shown in Figure 1. b), the transfer function concept is very useful. $G(z,t)$ in Figure 1. b) denotes the absorber impulse response, and is given by

$$g(z,t)=\frac{p_0}{2c_s}\begin{cases}A(z-c_s t) & z>0\\ A(z+c_s t) & z<0\end{cases} \tag{2}$$

where $A(z)$ is the spatial shape of the absorber, $r(t)$ is the receiver-filter impulse response. The signal received at the receiver-filter also contains noise $n(t)$ which is assumed to be a zero-mean additive Gaussian white noise [17] which is assumed to have a double-sided power spectral density of $\tilde{S}_{nn}(\omega)=\frac{N_0}{2}$. The output of receiver-filter $y(z,t)$ contains the photoacoustic signal $y_s(z,t)$ and the noise signal $y_n(z,t)$ and is given by

$$y(z,t)=y_s(z,t)+y_n(t) \tag{3}$$

where

$$\begin{aligned} &y_s(z,t)=r(t)*g(z,t)*I(t)\\ \text{or}\quad &\tilde{y}_s(z,\omega)=\tilde{R}(\omega)\tilde{G}(z,\omega)\tilde{I}(\omega)\end{aligned} \tag{4}$$

$$\begin{aligned} &y_n(t)=r(t)*n(t)\\ \text{or}\quad &\tilde{y}_n(\omega)=\tilde{R}(\omega)\tilde{S}_{nn}(\omega)\end{aligned} \tag{5}$$

Given a chosen waveform/receiver filter pair, the instantaneous signal-to-noise ratio (SNR) at time t_0 is defined as

$$SNR=\left(\frac{S}{N}\right)_{t_0}=\frac{\left|y_s(z,t_0)\right|^2}{E\left|y_n(t_0)\right|^2} \tag{6}$$

where $E\left|y_n(t_0)\right|$ refers to the noise expectation value.

III. Matched-Filter and the Chirp

Matched-filtering is a traditional way to improve SNR in radar technology, and the transfer function of the receiver-filter for the ideal matched-filter for any arbitrary input waveform $I(t)$ is given by [17]

$$\tilde{R}(\omega)=k\tilde{G}^*(z,\omega)\tilde{I}^*(\omega)e^{-i\omega t_0} \tag{7}$$

where k is a scaling constant. However, (7) is not necessarily implementable for a typical photoacoustic system since $\tilde{G}(z,\omega)$ (determined by the absorber profile) is not known apriori. In this case, the receiver-filter is implemented as

$$\tilde{R}(\omega)=k\tilde{I}^*(\omega)\,e^{-i\omega t_0} \tag{8}$$

Under the condition of (8), (4) becomes

$$\tilde{y}_s(z,\omega)=k\,\tilde{G}(z,\omega)\underbrace{\tilde{I}(\omega)\tilde{I}^*(\omega)}_{\tilde{I}^{SD}(\omega)}e^{-i\omega t_0} \tag{9}$$

In (9), k is simply a scaling factor and the $e^{-i\omega t_0}$ is just a time delay. Hence, (9) can be interpreted in input/output form as a pressure response to an input pulse $\tilde{I}^{SD}(\omega)$ where $\tilde{I}^{SD}(\omega)=\left|\tilde{I}(\omega)\right|^2$ is the spectral energy density of $I(t)$. The inverse Fourier transform of $\left|\tilde{I}(\omega)\right|^2$ in time domain is known to be

$$R_{II}(t)=\int_{-\infty}^{\infty} I(t+\tau)\overline{I(\tau)}\,d\tau \tag{10}$$

which is the autocorrelation of $I(t)$. The SNR in (6) can then be then written

$$SNR = \frac{\frac{1}{\pi}\left|\int_{-\infty}^{\infty} \tilde{G}(z,\omega)\left|\tilde{I}(\omega)\right|^2 d\omega\right|^2}{N_0 \int_{-\infty}^{\infty} \left|\tilde{I}(\omega)\right|^2 d\omega} \quad (11)$$

By implementing matched-filtering, the SNR is improved. However, $R_{II}(t)$ generally has a longer duration than $I(t)$, which may leads to a worse resolution. However, there exist classes of specific waveforms which possess the property of pulse compression, which means that the waveform will have shorter duration after autocorrelation. The chirp is one such waveform that can be compressed and is given by

$$I_T(t) = \begin{cases} \cos\left(2\pi f_0 t + \frac{\pi \Delta t^2}{T}\right) & |t| < \frac{T}{2} \\ 0 & |t| > \frac{T}{2} \end{cases} \quad (12)$$

where T is the duration of the chirp. During the T second interval of the pulse, the instantaneous frequency changes linearly from $(f_0 - KT/2)$ Hz to $(f_0 + KT/2)$ Hz. The sweep Δ is the difference in these two values. The $\left|\tilde{I}(\omega)\right|^2$ of the chirp shown in (11) can be approximated as a rectangular function and is given by [18]

$$\left|\tilde{I}_T(f)\right|^2 \approx \begin{cases} \frac{T}{4\Delta} & f_0 - \frac{\Delta}{2} \le f \le f_0 + \frac{\Delta}{2} \\ 0 & \text{otherwise} \end{cases} \quad (13)$$

IV. CHIRP PARAMETER EFFECTS ON SNR

From (11), it becomes clear that the SNR is determined by the absorber frequency spectrum that lies within the frequency interval bounded by the chirp sweep range $f_0 + \frac{\Delta}{2}$ and $f_0 - \frac{\Delta}{2}$. Now consider a simple bandlimited absorber. The bandlimited absorber is considered as a square function in the frequency domain as

$$\hat{A}(f) = \begin{cases} 1 & |f| \le \frac{\Delta_a}{2} \\ 0 & otherwise \end{cases} \quad (14)$$

Taking the chirp rectangular approximation shown in (13), the equation of SNR for a bandlimited absorber can be written as

$$SNR = \frac{TC}{\Delta^2} \times (Overlapping\ Area)^2 \quad (15)$$

where $C = \frac{p_0^2}{16\pi N_0 c_s^2}$ is a constant factor which is independent of the chirp, and the overlapping area is the shaded area shown in Figure 2. It is obvious from (15) that SNR is proportional to chirp duration *T*.

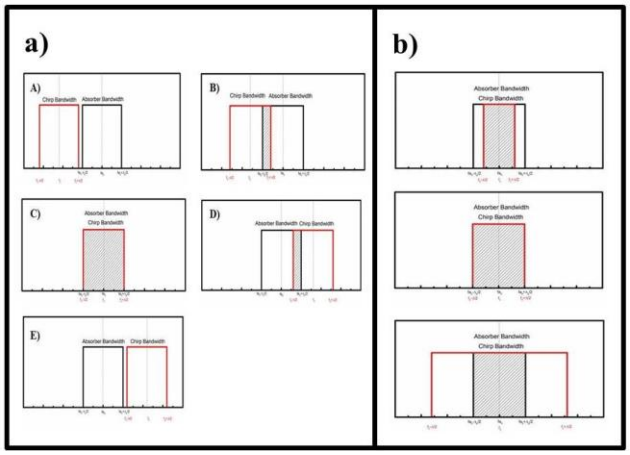

Figure 2. Bandlimited absorber and chirp frequency spectrum

In Figure 2. , the black boxes denote the bandlimited absorber frequency spectrum, and the red boxes denote the rectangular approximation of the chirp spectrum. Figure 2. a) shows that the chirp bandwidth Δ remains constant and the chirp center frequency f_0 moves from left to right of the absorber. The relationship between SNR and f_0 is shown in Figure 3. a). The SNR first increases with f_0 until a maximum value is reached and then decreases, corresponding to the overlapping conditions. Figure 2. b) visualize the overlapping conditions when the chirp center frequency remains constant and bandwidth increases. The trend of the SNR is shown in Figure 3. b). The overall trend is that SNR decreases with increasing chirp bandwidth, and the maximum value occurs when the chirp bandwidth is smaller or equal to the absorber bandwidth, $\Delta \le \Delta_a$.

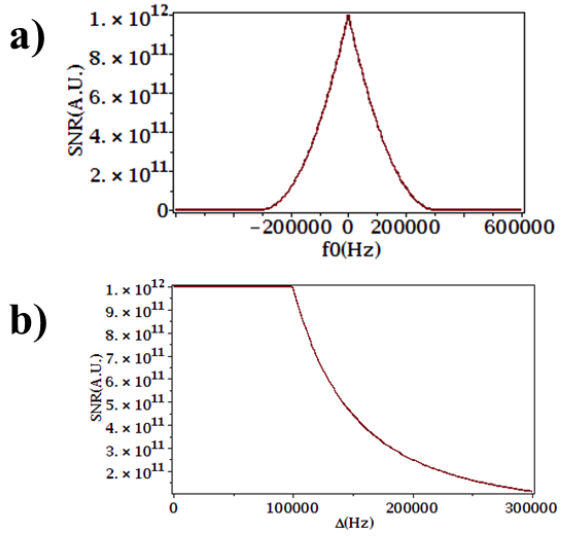

Figure 3. Bandlimited absorber and chirp frequency spectrum

In conclusion, by controlling the chirp parameters, the SNR for a photoacoustic radar signal can be optimized. In order to get a higher SNR, chirp duration T should be maximized, chirp center frequency f_0 should be controlled to make the chirp spectrum overlap with that of the absorber spectrum, and chirp bandwidth Δ should be smaller or equal to the absorber bandwidth.

ACKNOWLEDGMENT

This work was financially supported by the Natural Sciences and Engineering Research Council of Canada.

REFERENCES

[1] Y. Fan, A. Mandelis, G. Spirou, I. A. Vitkin, and W. M. Whelan, "Laser photothermoacoustic heterodyned lock-in depth profilometry in turbid tissue phantoms," *Phys. Rev. E*, vol. 72, no. 5, p. 051908, Nov. 2005.

[2] S. Telenkov and A. Mandelis, "Signal-to-noise analysis of biomedical photoacoustic measurements in time and frequency domains," *Rev. Sci. Instrum.*, vol. 81, no. 12, p. 124901, Dec. 2010.

[3] G. Ku and L. V. Wang, "Scanning thermoacoustic tomography in biological tissue," *Med. Phys.*, vol. 27, no. 5, pp. 1195–1202, May 2000.

[4] M. Xu and L. V. Wang, "Time-domain reconstruction for thermoacoustic tomography in a spherical geometry," *Med. Imaging IEEE Trans. On*, vol. 21, no. 7, pp. 814–822, 2002.

[5] M. Xu, Y. Xu, and L. V. Wang, "Time-domain reconstruction algorithms and numerical simulations for thermoacoustic tomography in various geometries," *IEEE Trans. Biomed. Eng.*, vol. 50, no. 9, pp. 1086–1099, Sep. 2003.

[6] A. A. Karabutov, N. B. Podymova, and V. S. Letokhov, "Time-resolved optoacoustic measurement of absorption of light by inhomogeneous media," *Appl. Opt.*, vol. 34, no. 9, pp. 1484–1487, Mar. 1995.

[7] S. A. Telenkov and A. Mandelis, "Photothermoacoustic imaging of biological tissues: maximum depth characterization comparison of time and frequency-domain measurements," *J. Biomed. Opt.*, vol. 14, no. 4, pp. 044025-044025-12, 2009.

[8] B. Lashkari and A. Mandelis, "Linear frequency modulation photoacoustic radar: Optimal bandwidth and signal-to-noise ratio for frequency-domain imaging of turbid media," *J. Acoust. Soc. Am.*, vol. 130, no. 3, pp. 1313–1324, Sep. 2011.

[9] B. Lashkari and A. Mandelis, "Comparison between pulsed laser and frequency-domain photoacoustic modalities: Signal-to-noise ratio, contrast, resolution, and maximum depth detectivity," *Rev. Sci. Instrum.*, vol. 82, no. 9, p. 094903, Sep. 2011.

[10] B. Lashkari and A. Mandelis, "Photoacoustic radar imaging signal-to-noise ratio, contrast, and resolution enhancement using nonlinear chirp modulation," *Opt. Lett.*, vol. 35, no. 10, pp. 1623–1625, May 2010.

[11] Y. Fan, A. Mandelis, G. Spirou, I. A. Vitkin, and W. M. Whelan, "Three-dimensional photothermoacoustic depth-profilometric imaging by use of a linear frequency sweep lock-in heterodyne method," 2004, vol. 5320, pp. 113–127.

[12] S. A. Telenkov, R. Alwi, and A. Mandelis, "Photoacoustic correlation signal-to-noise ratio enhancement by coherent averaging and optical waveform optimization," *Rev. Sci. Instrum.*, vol. 84, no. 10, p. 104907, Oct. 2013.

[13] B. Lashkari and A. Mandelis, "Features of the Frequency- and Time-Domain Photoacoustic Modalities," *Int. J. Thermophys.*, vol. 34, no. 8–9, pp. 1398–1404, 2013.

[14] N. Baddour and A. Mandelis, "The Effect of Acoustic Impedance on Subsurface Absorber Geometry Reconstruction using 1D Frequency-Domain Photoacoustics," *Photoacoustics*, vol. 3, no. 4, pp. 132–142, Dec. 2015.

[15] GeraldJ Diebold, "Photoacoustic Monopole Radiation," in *Photoacoustic Imaging and Spectroscopy*, 0 vols., CRC Press, 2009, pp. 3–17.

[16] M. Xu and L. V. Wang, "Photoacoustic imaging in biomedicine," *Rev. Sci. Instrum.*, vol. 77, no. 4, 2006.

[17] J. R. Klauder, A. C. Price, S. Darlington, and W. J. Albersheim, "The Theory and Design of Chirp Radars," *Bell Syst. Tech. J.*, vol. 39, no. 4, pp. 745–808, 1960.

[18] B. Lashkari, "Photoacoustic Imaging Using Chirp Technique: Comparison with Pulsed Laser Photoacoustics," Ph.D dissertation, University of Toronto, 2011.